Acidochromic organic photovoltaic integrated device

Chemical Engineering Journal 452 (2023) 139479

Contents lists available at ScienceDirect

Chemical Engineering Journal

journal homepage: www.elsevier.com/locate/cej

Acidochromic organic photovoltaic integrated device

Yufei Wang [a,1], Qiaonan Chen [a,b,c,1], Zhe Liu [a,d], Feng Yu [a], Wenyan Su [a,e], Zhizhao Cai [a], Wei Guan [a], Yaohui Li [a], Lan Sheng [c], Zhengjian Qi [d], Ergang Wang [b,*], Lintao Hou [a,*]

[a] Guangzhou Key Laboratory of Vacuum Coating Technologies and New Energy Materials, Siyuan Laboratory, Department of Physics, Jinan University, Guangzhou 510632, China
[b] Department of Chemistry and Chemical Engineering, Chalmers University of Technology, Göteborg SE-412 96, Sweden
[c] State Key Lab of Supramolecular Structure and Materials, College of Chemistry, Jilin University, Changchun 130012, China
[d] Jiangsu Province Hi-Tech Key Laboratory for Biomedical Research School of Chemistry and Chemical Engineering, Southeast University, Nanjing 211189, China
[e] School of Materials Science and Engineering, Xi'an University of Science and Technology, Xi'an 710054, China

ARTICLE INFO

Keywords:
Acidochromic
Organic solar cell
Integrated device
Ring-opening reaction
Acidification

ABSTRACT

Tremendous efforts have been devoted to boosting the power conversion efficiency (PCE) of organic solar cells (OSCs) via the introduction of cathode interlayers (CILs). However, CIL materials have limited diversity and the development of multifunctional devices is largely neglected. Herein, an acidochromic organic photovoltaic integrated device is firstly proposed by introducing an acid-sensitive stimulating-reaction organic molecule as both the CIL of OSCs and the sensor of monitoring environmental acidity. The oxazolidine unit of acidochromic molecule can form a ring-opening structure after acid treatment, resulting in the remarkable color change with the direct reflection of pH value of ecological environment. The additive-free PM6:Y6 OSCs using the acidochromic molecule as the CIL achieve an excellent PCE of above 15.29 %, which is 47 % higher than that of the control device. The PCE can even maintain above 92 % after treating CIL with various strong acids (pH = 1). Moreover, the color of acidified films and the degraded performance of acidified OSCs can be easily restored by alkaline treatment. The successful application of CIL in other highly efficient photovoltaic systems proves its good universality. This work triggers the promising application of acidochromic molecules in solar cells as CIL with the additional function of recognition of acid environment.

1. Introduction

Organic solar cells (OSCs), as an effective method to relieve the global energy crisis, have been extensively studied due to their fascinating advantages of light weight, bendability, low-cost solution processibility and semitransparency [1–5]. At present, tremendous efforts have been dedicated to improving OSC performance with power conversion efficiency (PCE) of up to 19%, suggesting the promise of commercialization of OSCs in the near future [6–13]. Beyond that, the future organic photovoltaic device could be smarter with multifunction that can meet diverse requirements with the ability of monitoring various environmental conditions such as UV exposure and acid rain pollution [14–16]. For example, the photochromic OSC was firstly proposed by Rene A. J. Janssen et al, whose device exhibited remarkable changes in color under UV light [17]; although a very low PCE below 0.5 % was achieved [18–19]. The chemical reactivity of non-fullerene acceptor under acidic or basic environment was recently discussed by Zhou et al, while the quantitative characterization of acidic environments was not achieved since the non-fullerene acceptors possess a high intrinsic stability under acidic condition [20]. Thus, the realization of high-performance integrated OSCs with both photovoltaic function and monitoring pH values of the acidic environment is challenging but very attractive.

For high-efficiency OSCs, cathode interface modification plays a vital role in charge transport and extraction. A series of interface materials had been successfully applied in OSCs as the cathode interlayer (CIL), which can be mainly divided into three categories: alkali-halide salt or metal oxides (LiF, ZnO, Al_2O_3, TiO_x, etc.) [21–23], conjugated/non-conjugated polymers (PFN, FTBTF-N, PEO, PEIE, etc.) or polyelectrolytes (PFN-Br, PDINT-F3NBr, etc.) [24–28], and water/alcohol-soluble small molecules (NDI-N, PDINN, etc.) [29–30]. Different from these CILs reported, recently a series of molecular switches based on

* Corresponding authors.
E-mail addresses: ergang@chalmers.se (E. Wang), thlt@jnu.edu.cn, thlt@jnu.edu.cn (L. Hou).
[1] These authors contributed equally to this work.

https://doi.org/10.1016/j.cej.2022.139479
Received 26 July 2022; Received in revised form 13 September 2022; Accepted 26 September 2022
Available online 29 September 2022

oxazolidine derivatives with good batch-to-batch reproducibility and easy purification attract more attention due to their unique and obvious response under multiple stimuli including light, temperature, force, and acid/base [31–33]. In principle, the conjugated unit with suitable energy levels should endow them with excellent ability of regulating charge transport and extraction as the CIL in OSCs as well. Thus, building an integrated device with an ultrathin oxazolidine layer as the CIL in OSCs and a thick oxazolidine layer as the acid stimulation sensor will greatly enrich the diversity of application of organic photovoltaic technology and surely open a new frontier for molecular species of OSC

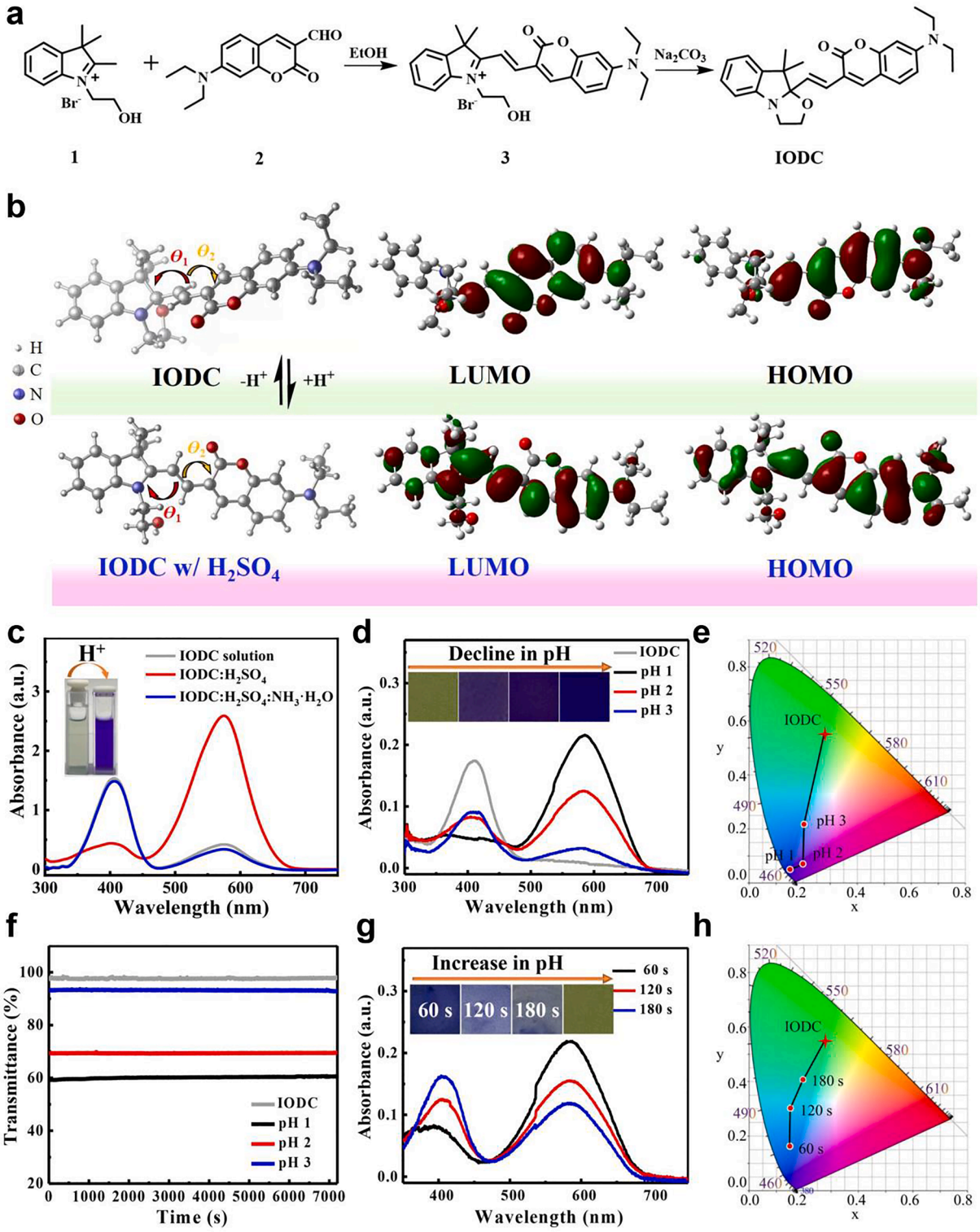

Fig. 1. (a) Synthesis route of IODC. (b) Optimized molecular geometries of the pristine and H_2SO_4-treated IODC with corresponding frontier molecular orbitals acquired from DFT calculations. (c) Absorption spectra of the IODC, IODC:H_2SO_4 (1:2, mol/mol), IODC:H_2SO_4:NH_3·H_2O (1:2:80, mol/mol) solutions. (d) Absorption spectra, (e) corresponding CIE color coordinates and (f) transmittance intensities at 580 nm for the IODC:HPC films w/o and w/ H_2SO_4 treatment over a pH range of 1 to 3. (g) Absorption spectra and (h) corresponding CIE color coordinates of the H_2SO_4-treated (pH = 1) IODC film in the reversible manner by using ammonia gas with different exposure time.

CILs. However, up to date, this kind of acidochromic organic photovoltaic integrated device has not been studied. The molecular structure design and the reason behind performance improvement should be explored.

Herein, an acidochromic organic photovoltaic integrated device was successfully fabricated for the first time using an acidochromic organic molecule (IODC, Fig. 1a) as both the CIL and the acid indicator. Due to the strong interactions between the H^+ of acids and the oxygen atoms with spare electron pairs in the five-membered ring of oxazolidine molecule of IODC, the ring-close oxazolidine isomer can turn to the ring-open isomer with the breaking of C—O bond after acid stimulation, which results in the fascinating color variation from light green to dark blue with increasing acid concentration. Thus, a sensitive response to changes of environmental acidity is successfully achieved with excellent stability and reproducibility. On the other hand, the PCE of OSCs with IODC as the CIL is greatly increased by 47% compared to the control device. Besides, the OSCs using IODC as the CIL exhibit an excellent tolerance to diverse acids with efficiencies maintaining more than 92% of the initial PCE, indicating this new type of acidochromic organic photovoltaic integrated device is very suitable for use in acidic conditions to both generate electrical power and monitor acid concentration of environment pollutants. Moreover, the changed color and deteriorated performance of acidochromic organic photovoltaic integrated device can be easily recovered by alkaline post-treatment. Furthermore, this new type of CIL is also suitable for other highly efficient OSCs and Perovskite solar cells (PSCs) with good universality. This very novel and unique work provides a new path for the wider commercial application of OSCs or PSCs in the future.

2. Results and discussion

2.1. Acidochromic mechanism

The concise synthesis route of IODC is shown in Fig. 1a with the related details listed in Supporting Information. The changes of molecular chemical structure and spatial conformation of IODC from ring-close to ring-open isomer induced by acid stimulation are depicted by density functional theory (DFT) calculations based on B3LYP/6-31G, as shown in Fig. 1b and Fig. S1, Supporting Information. The IODC molecule with a ring-close structure exhibits a quite planar conjugated backbone in the right side with the dihedral angle θ_2 of 1° between the vinyl unit and the 7-diethylamino-coumarin unit, compared to the dihedral angle θ_1 of 72° between the vinyl unit and the indole unit. Correspondingly, the highest occupied molecular orbital (HOMO) and lowest unoccupied molecular orbital (LUMO) of IODC are mainly delocalized over the vinyl and 7-diethylamino-coumarin parts. After acid stimulation, the planarity of IODC is further increased with the dihedral angles of 23° (θ_1) and 4° (θ_2), leading to electron cloud delocalization over the whole molecule backbone. The theoretical calculation results reveal that IODC should be an excellent electron transport material for OSCs when it is acidified by H_2SO_4 with increased planarity and conjugacy.

The strong interaction between the H^+ and the oxygen atom can break the C—O bond of five-membered ring of oxazolidine and form a new O—H bond through protonation, which results in significant absorption color variations (Fig. 1c). The chemical structure transformation of IODC by acid stimulation is confirmed experimentally by proton nuclear magnetic resonance (^{1}H NMR) spectroscopy, as shown in Fig. S2, Supporting Information. After adding a tiny droplet of H_2SO_4 into the IODC solution, a new set of proton signals are observed in the low-field ^{1}H NMR region with corresponding bond sites. The increased conjugation with the addition of electron-withdrawing unit after acidification causes a redshift of aromatic proton NMR signals. In other words, the ring-opening molecular structure has a larger positive charge (C═N^+) conjugation in the indole part, which leads to a larger molecular conjugation for the acidified molecule.

2.2. Acidochromic performance

The acidochromic characteristics of IODC dissolved in ethanol (EtOH) are investigated by UV–visible absorption spectroscopy. As shown in Fig. 1c, the main absorption peak at 407 nm with a light green color for the pristine IODC solution is shifted to 570 nm with a dark blue color for the H_2SO_4-treated IODC solution. The hydroxy propyl cellulose (HPC) with proper polarity is a good substrate material for keeping IODC initially colorless and displaying color changes after acid stimulation. By mixing IODC with HPC polymeric matrix, the thick acidochromic film with rich color variations can be easily fabricated, which is very attractive in practical use with less IODC consumption and easy module manufacturing. As shown in Fig. 1d, obvious color variations of thick IODC films are also found under different pH conditions (pH = 1, 2 and 3) due to the gradual changes of IODC structure from ring-closing to ring-opening. The photographs of thick IODC films after H_2SO_4 treating (pH = 1) and drying are displayed in Fig. S3, Supporting Information. The CIE coordinates of reflected light from the surface of IODC films are thus obviously changed from (0.28, 0.55) (IODC) to (0.15, 0.05) (pH = 1) (Fig. 1e). Apparently, the pH value or the concentration of H_2SO_4 can significantly affect the ring-opening extent of IODC. Moreover, it can be seen that the transmittance intensities of IODC films treated with different pH values of H_2SO_4 are nearly not changed with increasing time (Fig. 1f), indicating an excellent stability of acidochromic films in air. Indeed, the color of the acidified IODC solution or film can be easily recovered by $NH_3{\cdot}H_2O$ or ammonia gas, as shown in Fig. 1c,g,h, suggesting that it can be reused for acid detection with less material consumption. Moreover, the alkalified H_2SO_4:IODC sample also has very good stability in air with less change in absorption spectra after a period of time (Fig. S4). The color recovery process of the acidified IODC film via ammonia gas treatment is shown in Fig. S5, Supporting Information. The acidified IODC film can almost restore its initial color in just two minutes under the ammonia gas atmosphere at room temperature.

2.3. Cathode interlayer in acidochromic organic photovoltaic integrated device

The schematic diagram of the acidochromic organic photovoltaic integrated device structure using IODC as the CIL in OSCs and IODC:HPC as the acid sensor is shown in Fig. 2a. It can be seen that two different functions can be achieved on a single substrate. The color of the IODC:HPC film on the left can produce a fascinating change from light green to dark blue with the increase of acid concentrations like a pH test paper, while the device on the right can directly convert light to electricity. The photograph of the concrete acidochromic organic photovoltaic integrated device and the related molecular chemical structures are displayed in Fig. S6, Supporting Information. It can be seen that the fabrication process is very feasible for practical use (Fig. S7).

To analyze the effect of IODC as the CIL on carrier transport and charge extraction, the ultraviolet photoelectron spectroscopy (UPS) measurements for the bare Ag and IODC-treated Ag electrodes are carried out, as shown in Fig. 2c. The work function of the bare Ag electrode is 4.37 eV, which can be greatly reduced to 4.00 eV after IODC modification. We infer that an interface dipole should be formed between IODC and Ag due to their strong interaction, as the negative chemical shift of Ag 3d core level is observed in XPS (Fig. 2d). The amino group in the 7-diethylamino-coumarin unit of IODC molecule can provide lone pair electrons to Ag, resulting in the upshift of the vacuum level [34–36]. Thus, the energy level difference between the work function of Ag and the LUMO energy level of Y6 is greatly decreased to zero, which is very beneficial to electron extraction (Fig. 2b, Fig. S8 and Table S1, Supporting Information). Besides, the surface conductivity of the PM6:Y6 active layer is greatly improved by inserting IODC, which is also conducive to forming a good ohmic contact with the Ag electrode (Fig. S9a-b, Supporting Information). It can be seen that the IODC molecules are evenly distributed over the PM6:Y6 active layer with

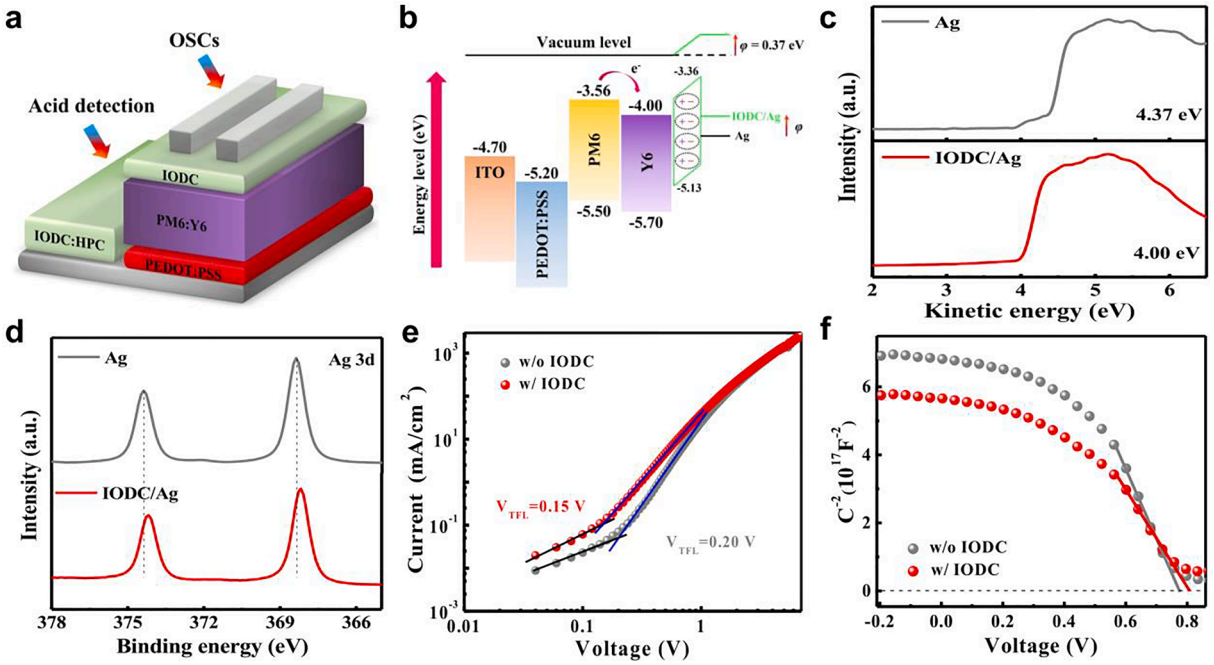

Fig. 2. (a) Schematic diagram of integrated structure of acidochromic OSCs. (b) Energy level diagram of OSCs. (c) UPS and (d) XPS spectra of the pure Ag and IODC-modified Ag. (e) $J-V$ curves of electron-only devices w/ and w/o IODC. (f) Mott-Schottky curves of OSCs w/ and w/o IODC.

negligible roughness changes (1.47 vs 1.59 nm) (Fig. S9c-d, Supporting Information). The good compatibility of two adjacent layers is related to their similar surface energies (Fig. S10, Tables S2 and S3, Supporting Information), which is in favor of forming better interface contact.

2.4. Enhanced mobility and built-in potential

In addition to facilitating electron extraction, the improved electron transport property in the IODC-treated PM6:Y6 film is quantitatively evaluated according to space-charge limited current (SCLC) technique (Fig. 2e). The structures of electron-only device w/ and w/o IODC are ITO/ZnO/PM6:Y6/Ag and ITO/ZnO/PM6:Y6/IODC/Ag, respectively. The calculated electron mobility based on the Mott − Gurney law ($J = \frac{9\varepsilon_0\varepsilon_r\mu V^2}{8d^3}$) is 6.66×10^{-4} $cm^2\ V^{-1}\ s^{-1}$ for the IODC-modified PM6:Y6 film, which is much higher than 7.20×10^{-5} $cm^2\ V^{-1}\ s^{-1}$ for the pure PM6:Y6 film [37–38]. The higher electron mobility reveals that IODC interlayer can effectively boost electron transfer in PM6:Y6 based solar cells. Furthermore, the trap density (N_t) of electron-only devices can be extracted by $N_t = \frac{2\varepsilon_0\varepsilon_r V_{TFL}}{qL^2}$, where V_{TFL} denotes the trap-filled limit voltage. The calculated total trap densities of electron-only devices are 3.47×10^{17} cm^{-3} (w/ IODC) and 4.60×10^{17} cm^{-3} (w/o IODC), respectively. The lower trap density indicates that the ultrathin IODC interlayer can passivate surface defects of PM6:Y6 active layer and accelerate electron transfer to the Ag electrode.

Except the above advantages listed, the IODC interlayer can also enhance the built-in potential (V_{bi}) of OSCs and reduce the coulomb capture radius (R_C) of photogenerated free hole-electron pairs. The Mott-Schottky curves of OSCs w/o or w/ IODC are tested to analyze the influence of IODC on V_{bi}, as shown in Fig. 2f and Table S4, Supporting Information. The V_{bi}, relative dielectric constant (ε_r) and carrier density (N_D) are extracted based on the equation of $\frac{1}{C^2} = \frac{2(V_{bi}-V)}{A^2 e\varepsilon_0\varepsilon_r N_D}$ [39–40]. Remarkably, a high V_{bi} value of 0.81 V is obtained for the IODC-based OSC compared to 0.77 V for the control OSC without IODC. Besides, the ε_r (5.64) and N_D (1.10×10^{16} cm^{-3}) of the IODC-based OSC are much higher than those (4.66 and 0.92×10^{16} cm^{-3}) of the control OSC without IODC, respectively, due to the ameliorative electron transport and extraction [41]. Furthermore, the R_C of excitons can be obtained according to the equation: $R_c = \frac{e^2}{4\pi\varepsilon_0\varepsilon_r kT}$ [42–43]. A smaller R_C of 9.88 nm for the IODC-based OSC than 11.96 nm for the control OSC indicates that hole-electron pair can be separated more easily in the diffusion process by overcoming their coulomb interaction under the circumstance of the insertion of IODC. Thus, a higher short current density (J_{SC}) can be achieved in the IODC-based OSC.

2.5. Device performance and analysis

The OSC is fabricated based on a typical device structure of ITO/PEDOT:PSS/ PM6:Y6/CIL/Ag, where the PM6:Y6 layer is directly formed by spin-coating without adding any additives or treatments. The control OSCs w/o CIL or w/ a commercial CIL of PFN-Br are also fabricated for comparison. Fig. 3a presents the current density–voltage ($J-V$) curves of OSCs w/ and w/o the IODC CIL. A poor PCE of 10.41 % is obtained for the OSC w/o IODC. In contrast, a much higher PCE of 15.29 % is achieved for the IODC-based OSC, which can be ascribed to the increase of open circuit voltage (V_{OC}) from 0.78 to 0.85 V, J_{SC} from 22.62 to 24.88 mA cm^{-2}, and fill factor (FF) from 59.00 to 72.30 % (Table 1). Meanwhile, another device with PFN-Br as the control CIL exhibits a relatively low PCE of 14.53 % (Fig. S11, Supporting Information), due to the larger series resistance and smaller shunt resistance [44]. The external quantum efficiency (EQE) spectra of OSCs are characterized and displayed in Fig. 3b. The small deviation below 5% is acquired between the measured J_{SC} from $J-V$ curves and the extracted J_{SC} from EQE spectra, suggesting that the J_{SC} value is credible. Meanwhile, the dark current below 0.80 V for the IODC-based OSC is greatly decreased compared with the control OSC w/o IODC (Fig. 3c), which attributes to the increase in V_{OC} (0.85 vs 0.78 V) [28,45–46]. Here we emphasize that the PCE remains nearly constant over a wide range of IODC thicknesses (Fig. S12 and Table S5, Supporting Information), indicating it is well suited for the OSC mass production.

The time-resolved photocurrent is measured by the photo-induced charge extraction linearly increasing voltage (photo-CELIV) for revealing the influence of IODC interlayer on average carrier mobility (μ_{avg}) in OSCs (Fig. 3d) [47], which is extracted based on the equation $\mu_{avg} = 2d^2/(3At_{max}^2(1 + 0.36\Delta j/j_0))$. Evidently, the μ_{avg} is effectively

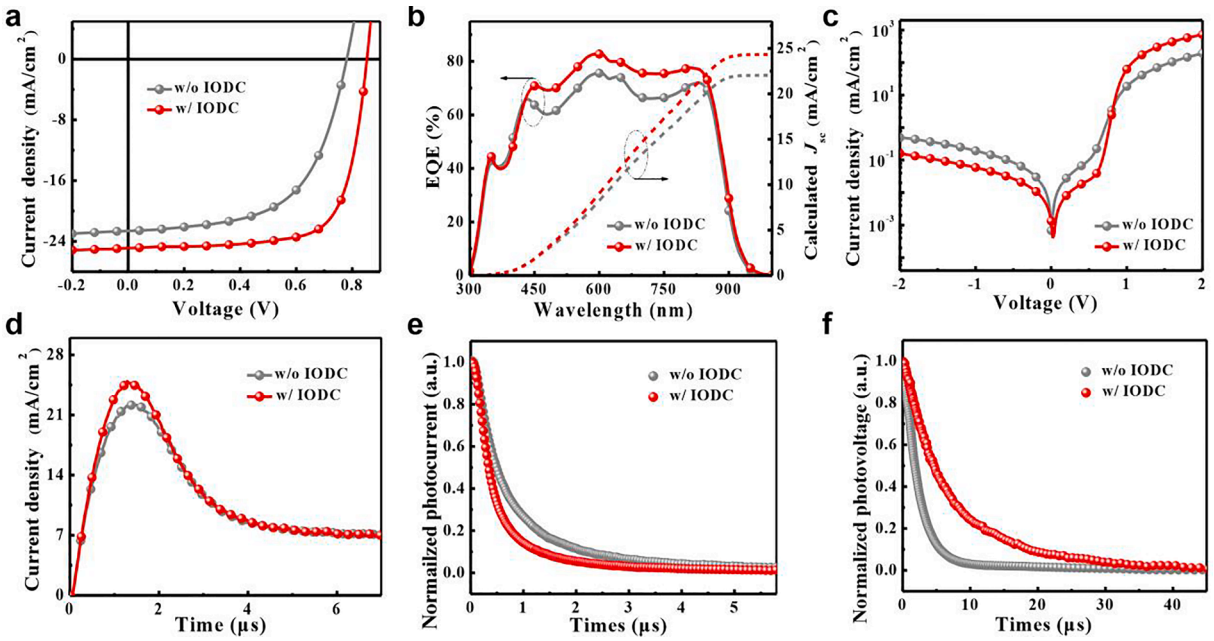

Fig. 3. (a) $J-V$, (b) EQE, (c) dark current, (d) photo-CELIV, (e) TPC and (f) TPV curves of OSCs w/ and w/o the IODC CIL.

Table 1
Photovoltaic performance of OSCs w/o and w/ IODC, or w/ PFN-Br as the control CIL.

CIL	V_{OC} (V)	J_{SC} (mA cm^{-2})	FF (%)	PCE (%)[b]	R_s (Ω cm^{-2})	R_{sh} (Ω·cm^{-2})
w/o IODC	0.78 ± 0.01	22.62 ± 0.18 (22.05)[a]	59.00 ± 0.16	10.41 ± 0.11	5.68	654.12
w/ IODC	0.85 ± 0.02	24.88 ± 0.14 (24.33)[a]	72.30 ± 0.18	15.29 ± 0.14	2.94	1091.11
w/ PFN-Br	0.85 ± 0.01	24.10 ± 0.21	70.93 ± 0.04	14.53 ± 0.09	3.29	1015.49

[a] The integrated J_{SC} values are obtained from the EQE spectra.
[b] The average values are acquired from the 10 separated devices.

increased from 1.50×10^{-4} to 1.89×10^{-4} cm^2 V^{-1}s^{-1}, which is mainly related to the increase of electron mobility after the introduction of IODC (Fig. 2e). Furthermore, performance differences are reflected in the results of impedance spectroscopy (Fig. S13 and Table S6, Supporting Information). Obviously, a small series resistance of R_3 (26.84 Ω) is acquired for the IODC-based OSC comparing to 59.18 Ω for the control OSC without IODC, which in turn seriously affects the FF value increased from 59.00 to 72.30 %. R_1 decreases from 943.5 to 563.1 Ω when the IODC interlayer is introduced between the PM6:Y6 and Ag electrode, which is consistent with the results of better interface contact in Fig. S9a,b, Supporting Information. The decrease of R_2 means that finer donor/acceptor phase separation coming from low intersolubility could be formed after spin-coating the IODC layer [48]. For further exploring the dynamic impact of IODC on carrier lifetime and extraction, the transient photocurrent (TPC) and transient photovoltage (TPV) curves of OSCs w/o or w/ IODC are measured, respectively (Fig. 3e-f). After the IODC interlayer is introduced, the charge extraction time is greatly accelerated from 0.70 to 0.44 μs. Meanwhile, the prolonged carrier lifetime of 6.49 μs is achieved in the IODC-based OSC compared with 2.35 μs for the OSC w/o IODC, indicating carrier loss coming from bimolecular and trap-assisted recombinations is notably suppressed [41].

2.6. Acidification and alkalization

Amazingly, even when the IODC layer is acidified by different types of acids, the OSCs still can keep good photovoltaic performance. The PCEs of OSCs can remain 92 ~ 98 % of initial value after IODC is acidified with different organic or inorganic acids, such as CH_3COOH (pH = 3), HCl (pH = 1), HNO_3 (pH = 1) and H_2SO_4 (pH = 1) (Fig. 4a,d, Table S7). This is very favorable to practical applications, since device stability may be problematic in an acidic environment. Especially, the OSC shows the best tolerance to the sulfuric acid (H_2SO_4), which is the main component of acid rain. The tiny decline about 2% in efficiency may come from the excessive work function elevation of Ag electrode by the H_2SO_4-acidified IODC (Fig. S14, Supporting Information). Furthermore, the PCE of photovoltaic device can still reach more than 14.41 % even when the volume ratio of H_2SO_4 (pH = 1) to IODC is up to 4:100 (Fig. 4b,e, Table S8). However, in case of the H_2SO_4/IODC volume ratio up to 8:100, the device performance begins to deteriorate, which might originate from the excessive residual hydrogen ions as the trapping sites [20]. The stability of IODC-based OSCs w/o and w/ acidification measured under a nitrogen atmosphere without encapsulation is shown in Fig. S15. The results indicate that the device stability is slightly reduced after IODC acidification, in which the H_2SO_4-treated IODC based OSC has a relatively good stability when compared with other organic or inorganic acids-treated IODC based devices.

With similarity to the color recovery of acidified IODC films by ammonia gas, the performance of H_2SO_4-acidified OSCs can also be recovered to initial value after ammonium hydroxide treatment. By increasing volume ratio of $NH_3{\cdot}H_2O$ (pH = 11) to H_2SO_4-acidified IODC (8:100 vol/vol), it can be seen that the PCE is greatly improved from 10.77 % to 15.37 % (16:8:100 vol/vol) (Fig. 4c,f, Table S8), due to gradual reverse changes of IODC structure from ring-opening to ring-closing. The excellent tolerance of IODC CIL to acids or bases provides a possibility for OSC to work under harsh acidic or basic conditions. In addition, the reversible change of photovoltaic performance of the IODC-based unencapsulated OSCs is directly verified by using acid

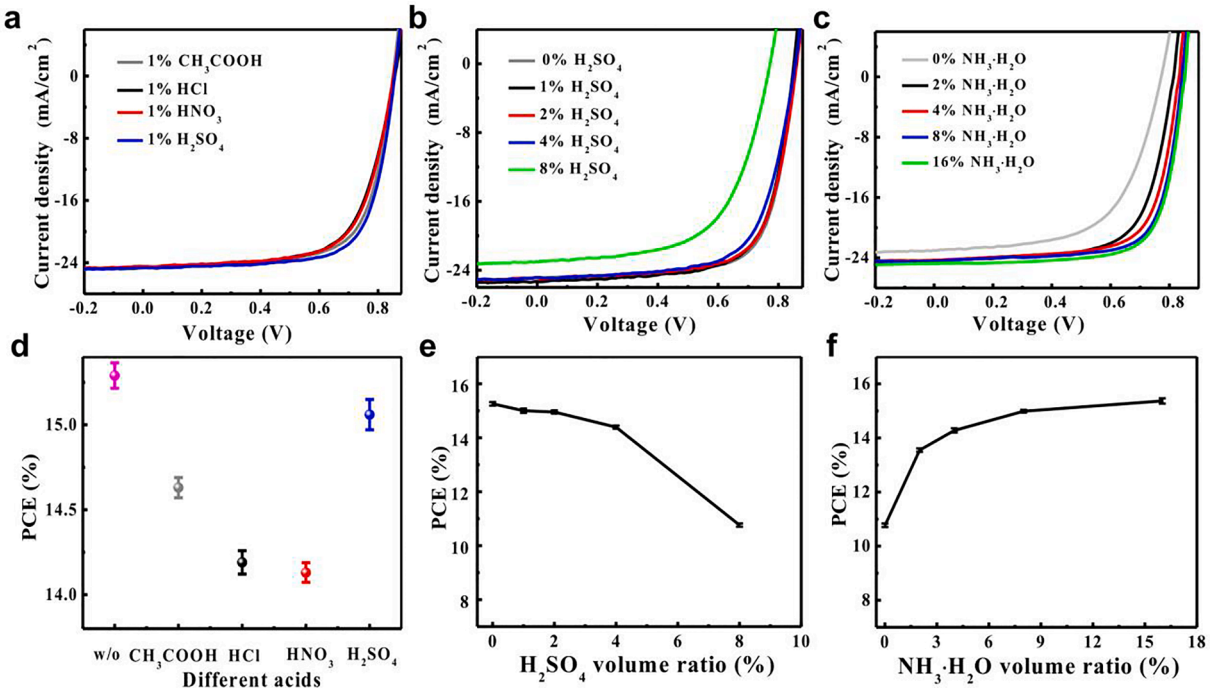

Fig. 4. (a) $J-V$ curves and (d) statistical PCEs of IODC-based OSCs acidified with different types of acids (acid/IODC (1 mg mL^{-1}) = 1:100 vol/vol). (b) $J-V$ curves and (e) statistical PCEs of IODC-based OSCs acidified with different volume ratios of H_2SO_4 (pH = 1) to IODC (1 mg mL^{-1}). (c) $J-V$ curves and (f) statistical PCEs of H_2SO_4-acidified (8 % H_2SO_4) OSCs recovered using different volume ratios of $NH_3{\cdot}H_2O$ (pH = 11) to IODC (1 mg mL^{-1}).

corrosion and base recovery (Fig. S16 and Table S9, Supporting Information). The fact that the PCE can be easily improved by ~ 18.8 % (11.54 % vs 13.71 %) demonstrates that the alkalization method has great practical value in recovery of efficiency. Furthermore, we speculate that if the deteriorated Ag electrode was removed and replaced by fresh metal electrode, the PCE should be increased to the initial value [49]. For other active systems like PM6:L8-BO and $CsFAMAPbI_3$, higher PCEs above 16.72 % are also obtained after using IODC as the CIL (Fig. S17a,b, Table S10, Supporting Information), verifying a general applicability of this novel acidochromic cathode interlayer in different types of solar cells.

3. Conclusions

In this paper, for the first time we propose an attractive acidochromic organic photovoltaic integrated device based on an acidochromic organic molecule with dual functions of acid indicator and CIL for solar cells. By controlling the C—O bond breaking and C═N^+ bond forming reactions in the oxazolidine unit with the assistance of hydrogen ions in acid, the main absorption peak of IODC is greatly shifted with displaying fascinating acidochromic features. The superior stability and good reproducibility of acidochromic films ensure sensitive and reliable detection of environmental acidity. Besides, the strong conjugacy in conjunction with a large dipole effect from the 7-diethylamino-coumarin unit can increase the electron transport and extraction in OSCs. Compared with the control device without IODC CIL, the PCE of the device with IODC is greatly increased by 47%. Interestingly it can retain more than 92% of the original value even if the IODC interlayer is acidified by organic or inorganic acids. Likewise, the deteriorated PCE of sulphuric acid heavy doping OSCs can also be recovered by ammonium hydroxide post-treatment, which is very attractive in practical use with less material consumption. Moreover, this novel type of CIL is generally applicable in various photovoltaic systems. This work demonstrates the feasibility of preparing acidochromic organic photovoltaic integrated device and surely promotes the diversity of CIL for OSCs.

Declaration of Competing Interest

The authors declare that they have no known competing financial interests or personal relationships that could have appeared to influence the work reported in this paper.

Data availability

Data will be made available on request.

Acknowledgements

Y.W. and Q.C. contributed equally to this work. This work was supported by National Natural Science Foundation of China Projects (61774077, 22005121), Key Projects of Joint Fund of Basic and Applied Basic Research Fund of Guangdong Province (2019B1515120073, 2019B090921002, 2020A1414010036), High-End Foreign Experts Project (G20200019046), Research Fund of Guangdong-Hong Kong-Macao Joint Laboratory for Intelligent Micro-Nano Optoelectronic Technology (No. 2020B1212030010) and Guangzhou Key laboratory of Vacuum Coating Technologies and New Energy Materials Open Projects Fund (KFVE20200006). L.S. thanks the National Science Foundation of China (21975099) and the Fundamental Research Funds for the Central Universities for their financial support. The authors thanks Dr. Yu-Mo Zhang, Jilin University, for his assistance in theoretical calculations. E. W. acknowledges the financial support from the K&A Wallenberg Foundation (2017.0186, 2016.0059), the Swedish Energy Agency, the Swedish Research Council (2016-06146, 2019-02345), and Formas.

Appendix A. Supplementary data

Supplementary data to this article can be found online at https://doi.org/10.1016/j.cej.2022.139479.

References

[1] H. Wang, H. Lu, Y.-N. Chen, A. Zhang, Y. Liu, D. Li, Y. Liu, X. Xu, Z. Bo, A versatile planar building block with C_{2V} symmetry for high-performance non-halogenated solvent processable polymer donors, Adv. Energy Mater. 12 (16) (2022) 2104028.

[2] Y. Su, L. Zhang, Z. Ding, Y. Zhang, Y. Wu, Y. Duan, Q. Zhang, J. Zhang, Y. Han, Z. Xu, R. Zhang, K. Zhao, S. Liu, Carrier generation engineering toward 18% efficiency organic solar cells by controlling film microstructure, Adv. Energy Mater. 12 (19) (2022) 2103940.

[3] J. Jing, S. Dong, K. Zhang, Z. Zhou, Q. Xue, Y. Song, Z. Du, M. Ren, F. Huang, Semitransparent organic solar cells with efficiency surpassing 15%, Adv. Energy Mater. 12 (20) (2022) 2200453.

[4] T. Zhang, C. An, P. Bi, Q. Lv, J. Qin, L. Hong, Y. Cui, S. Zhang, J. Hou, A thiadiazole-based conjugated polymer with ultradeep HOMO level and strong electroluminescence enables 18.6% efficiency in organic solar cell, Adv. Energy Mater. 11 (35) (2021) 2101705.

[5] W. Feng, S. Wu, H. Chen, L. Meng, F. Huang, H. Liang, J. Zhang, Z. Wei, X. Wan, C. Li, Z. Yao, Y. Chen, Tuning morphology of active layer by using a wide bandgap oligomer-like donor enables organic solar cells with Over 18% efficiency, Adv. Energy Mater. 12 (16) (2021) 2104060.

[6] R. Ma, C. Yan, P.-W.-K. Fong, J. Yu, H. Liu, J. Yin, J. Huang, X. Lu, H. Yan, G. Li, In situ and ex situ investigations on ternary strategy and co-solvent effects towards high-efficiency organic solar cells, Energy Environ. Sci. 15 (6) (2022) 2479–2488.

[7] R. Ma, C. Yan, J. Yu, T. Liu, H. Liu, Y. Liu, J. Chen, Z. Luo, B. Tang, X. Lu, G. Li, H. Yan, High-efficiency ternary organic solar cells with a good figure-of-merit enabled by two low-cost donor polymers, ACS Energy Lett. 7 (8) (2022) 2547–2556.

[8] T. Liu, W. Gao, G. Zhang, L. Zhang, J. Xin, W. Ma, C. Yang, H. Yan, C. Zhan, J. Yao, A high-performance non-fullerene acceptor compatible with polymers with different bandgaps for efficient organic solar cells, Solar RRL 3 (5) (2019) 1800376.

[9] T. Liu, W. Gao, Y. Wang, T. Yang, R. Ma, G. Zhang, C. Zhong, W. Ma, H. Yan, C. Yang, Unconjugated side-chain engineering enables small molecular acceptors for highly efficient non-fullerene organic solar cells: insights into the fine-tuning of acceptor properties and micromorphology, Adv. Funct. Mater. 29 (26) (2019) 1902155.

[10] K. Jin, Z. Xiao, L. Ding, 18.69% PCE from organic solar cells, J. Semicond. 42 (6) (2021), 060502.

[11] F. Liu, L. Zhou, W. Liu, Z. Zhou, Q. Yue, W. Zheng, R. Sun, W. Liu, S. Xu, H. Fan, L. Feng, Y. Yi, W. Zhang, X. Zhu, Organic solar cells with 18% efficiency enabled by an alloy acceptor: a two-in-one strategy, Adv. Mater. 33 (27) (2021) 2100830.

[12] Q. Liu, Y. Jiang, K. Jin, J. Qin, J. Xu, W. Li, J. Xiong, J. Liu, Z. Xiao, K. Sun, S. Yang, X. Zhang, L. Ding, 18% Efficiency organic solar cells, Sci. Bull. 65 (4) (2020) 272–275.

[13] K.-E. Hung, Y.-S. Lin, Y.-J. Xue, H.-R. Yang, Y.-Y. Lai, J.-W. Chang, C.-J. Su, A.-C. Su, C.-S. Hsu, U.-S. Jeng, Y.-J. Cheng, Non-volatile perfluorophenyl-based additive for enhanced efficiency and thermal stability of nonfullerene organic solar cells via supramolecular fluorinated interactions, Adv. Energy Mater. 12 (12) (2022) 2103702.

[14] Q. Huaulmé, V.M. Mwalukuku, D. Joly, J. Liotier, Y. Kervella, P. Maldivi, S. Narbey, F. Oswald, A.J. Riquelme, J.A. Anta, R. Demadrille, Photochromic dye-sensitized solar cells with light-driven adjustable optical transmission and power conversion efficiency, Nat. Energy 5 (6) (2020) 468–477.

[15] J. Lin, M. Lai, L. Dou, C.S. Kley, H. Chen, F. Peng, J. Sun, D. Lu, S.A. Hawks, C. Xie, F. Cui, A.P. Alivisatos, D.T. Limmer, P. Yang, Thermochromic halide perovskite solar cells, Nat. Mater. 17 (3) (2018) 261–267.

[16] H. Xiao, P. Dang, X. Yun, G. Li, Y. Wei, Y. Wei, X. Xiao, Y. Zhao, M.S. Molokeev, Z. Cheng, J. Lin, Solvatochromic photoluminescent effects in all-inorganic manganese(II)-based perovskites by highly selective solvent-induced crystal-to-crystal phase transformations, Angew. Chem., Int. Ed. 60 (7) (2021) 3699–3707.

[17] B.W.H. Saes, M.M. Wienk, R.A.J. Janssen, Photochromic organic solar cells based on diarylethenes, RSC Adv. 10 (50) (2020) 30176–30185.

[18] B. Kan, M. Li, Q. Zhang, F. Liu, X. Wan, Y. Wang, W. Ni, G. Long, X. Yang, H. Feng, Y. Zuo, M. Zhang, F. Huang, Y. Cao, T.P. Russell, Y. Chen, A series of simple oligomer-like small molecules based on oligothiophenes for solution-processed solar cells with high efficiency, J. Am. Chem. Soc. 137 (11) (2015) 3886–3893.

[19] J.-D. Chen, C. Cui, Y.-Q. Li, L. Zhou, Q.-D. Ou, C. Li, Y. Li, J.-X. Tang, Single-junction polymer solar cells exceeding 10% power conversion efficiency, Adv. Mater. 27 (6) (2015) 1035–1041.

[20] X. Zhu, L. Hu, W. Wang, X. Jiang, L. Hu, Y. Zhou, Reversible chemical reactivity of non-fullerene acceptors for organic solar cells under acidic and basic environment, ACS Appl. Energy Mater. 2 (10) (2019) 7602–7608.

[21] D. Gao, M.G. Helander, Z.-B. Wang, D.P. Puzzo, M.T. Greiner, Z.-H. Lu, C_{60}:LiF blocking layer for environmentally stable bulk heterojunction solar cells, Adv. Mater. 22 (47) (2010) 5404–5408.

[22] S. Trost, K. Zilberberg, A. Behrendt, A. Polywka, P. Görrn, P. Reckers, J. Maibach, T. Mayer, T. Riedl, Overcoming the "light-soaking" issue in inverted organic solar cells by the use of Al:ZnO electron extraction layers, Adv. Energy Mater. 3 (11) (2013) 1437–1444.

[23] A. Guerrero, S. Chambon, L. Hirsch, G. Garcia-Belmonte, Light-modulated TiO_x interlayer dipole and contact activation in organic solar cell cathodes, Adv. Funct. Mater. 24 (39) (2014) 6234–6240.

[24] F. Huang, H. Wu, D. Wang, W. Yang, Y. Cao, Novel electroluminescent conjugated polyelectrolytes based on polyfluorene, Chem. Mater. 16 (4) (2004) 708–716.

[25] W. Zhang, Y. Wu, Q. Bao, F. Gao, J. Fang, Morphological control for highly efficient inverted polymer solar cells via the backbone design of cathode interlayer materials, Adv. Energy Mater. 4 (12) (2014) 1400359.

[26] F. Zhang, M. Ceder, O. Inganäs, Enhancing the photovoltage of polymer solar cells by using a modified cathode, Adv. Mater. 19 (14) (2007) 1835–1838.

[27] Y. Zhou, C. Fuentes-Hernandez, J. Shim, J. Meyer, A.J. Giordano, H. Li, P. Winget, T. Papadopoulos, H. Cheun, J. Kim, M. Fenoll, A. Dindar, W. Haske, E. Najafabadi, T.M. Khan, H. Sojoudi, S. Barlow, S. Graham, J.-L. Brédas, S.R. Marder, A. Kahn, B. Kippelen, A universal method to produce low-work function electrodes for organic electronics, Science 336 (6079) (2012) 327–332.

[28] Z. Wu, C. Sun, S. Dong, X.-F. Jiang, S. Wu, H. Wu, H.-L. Yip, F. Huang, Y. Cao, n-Type water/alcohol-soluble naphthalene diimide-based conjugated polymers for high-performance polymer solar cells, J. Am. Chem. Soc. 138 (6) (2016) 2004–2013.

[29] J. Yao, B. Qiu, Z.-G. Zhang, L. Xue, R. Wang, C. Zhang, S. Chen, Q. Zhou, C. Sun, C. Yang, M. Xiao, L. Meng, Y. Li, Cathode engineering with perylene-diimide interlayer enabling over 17% efficiency single-junction organic solar cells, Nat. Commun. 11 (2020) 2726.

[30] Q. Kang, L. Ye, B. Xu, C. An, S.J. Stuard, S. Zhang, H. Yao, H. Ade, J. Hou, A printable organic cathode interlayer enables over 13% efficiency for 1-cm^2 organic solar cells, Joule 3 (1) (2019) 227–239.

[31] M. Yoo, S. Park, H.-J. Kim, Activatable colorimetric and fluorogenic probe for fluoride detection by oxazoloindole-to-hydroxyethylindolium transformation, RSC Adv. 6 (24) (2016) 19910–19915.

[32] S. Zhu, M. Li, L. Sheng, P. Chen, Y. Zhang, S.-X.-A. Zhang, A spirooxazine derivative as a highly sensitive cyanide sensor by means of UV-visible difference spectroscopy, Analyst 137 (23) (2012) 5581–5585.

[33] L. Sheng, M. Li, S. Zhu, H. Li, G. Xi, Y.-G. Li, Y. Wang, Q. Li, S. Liang, K. Zhong, S.-X.-A. Zhang, Hydrochromic molecular switches for water-jet rewritable paper, Nat. Commun. 5 (2014) 3044.

[34] H. Back, G. Kim, J. Kim, J. Kong, T.K. Kim, H. Kang, H. Kim, J. Lee, S. Lee, K. Lee, Achieving long-term stable perovskite solar cells via ion neutralization, Energy Environ. Sci. 9 (4) (2016) 1258–1263.

[35] L. Duan, P. Wang, X. Yu, X. Han, Y. Chen, P. Zhao, D. Li, R. Yao, The synthesis and characterization of Ag-N dual-doped p-type ZnO: experiment and theory, Phys. Chem. Chem. Phys. 16 (9) (2014) 4092–4097.

[36] W. Li, C. Kong, G. Qin, H. Ruan, L. Fang, p-Type conductivity and stability of Ag–N codoped ZnO thin films, J. Alloys Compd. 609 (2014) 173–177.

[37] C. Melzer, E.J. Koop, V.D. Mihailetchi, P.W.M. Blom, Hole transport in poly (phenylene vinylene)/methanofullerene bulk-heterojunction solar cells, Adv. Funct. Mater. 14 (9) (2004) 865–870.

[38] M.-Y. Chiu, U.S. Jeng, M.-S. Su, K.-H. Wei, Morphologies of self-organizing regioregular conjugated polymer/fullerene aggregates in thin film solar cells, Macromolecules 43 (1) (2009) 428–432.

[39] T. Schiros, G. Kladnik, D. Prezzi, A. Ferretti, G. Olivieri, A. Cossaro, L. Floreano, A. Verdini, C. Schenck, M. Cox, A.A. Gorodetsky, K. Plunkett, D. Delongchamp, C. Nuckolls, A. Morgante, D. Cvetko, I. Kymissis, Donor-acceptor shape matching drives performance in photovoltaics, Adv. Energy Mater. 3 (7) (2013) 894–902.

[40] C. Zhan, X. Zhang, J. Yao, New advances in non-fullerene acceptor based organic solar cells, RSC Adv. 5 (113) (2015) 93002–93026.

[41] C. Liu, D. Zhang, Z. Li, X. Zhang, W. Guo, L. Zhang, L. Shen, S. Ruan, Y. Long, Boosted electron transport and enlarged built-in potential by eliminating the interface barrier in organic solar cells, ACS Appl. Mater. Interfaces 9 (10) (2017) 8830–8837.

[42] K.M. Pelzer, S.B. Darling, Charge generation in organic photovoltaics: a review of theory and computation, Mol. Syst. Des. Eng. 1 (1) (2016) 10–24.

[43] M.B. Upama, N.K. Elumalai, M.A. Mahmud, M. Wright, D. Wang, C. Xu, A. Uddin, Effect of annealing dependent blend morphology and dielectric properties on the performance and stability of non-fullerene organic solar cells, Sol. Energy Mater. Sol. Cells 176 (2018) 109–118.

[44] W. Yu, L. Huang, D. Yang, P. Fu, L. Zhou, J. Zhang, C. Li, Efficiency exceeding 10% for inverted polymer solar cells with a ZnO/ionic liquid combined cathode interfacial layer, J. Mater. Chem. A 3 (20) (2015) 10660–10665.

[45] T. Yang, M. Wang, C. Duan, X. Hu, L. Huang, J. Peng, F. Huang, X. Gong, Inverted polymer solar cells with 8.4% efficiency by conjugated polyelectrolyte, Energy Environ. Sci. 5 (8) (2012) 8208–8214.

[46] J. Luo, H. Wu, C. He, A. Li, W. Yang, Y. Cao, Enhanced open-circuit voltage in polymer solar cells, Appl. Phys. Lett. 95 (2009), 043301.

[47] R.-Z. Liang, M. Babics, V. Savikhin, W. Zhang, V.M. Le Corre, S. Lopatin, Z. Kan, Y. Firdaus, S. Liu, I. McCulloch, M.F. Toney, P.M. Beaujuge, Carrier transport and recombination in efficient "all-small-molecule" solar cells with the nonfullerene acceptor IDTBR, Adv. Energy Mater. 8 (19) (2018) 1800264.

[48] Y. Lin, C. Cai, Y. Zhang, W. Zheng, J. Yang, E. Wang, L. Hou, Study of ITO-free roll-to-roll compatible polymer solar cells using the one-step doctor blading technique, J. Mater. Chem. A 5 (8) (2017) 4093–4102.

[49] R. Hu, X. Su, H. Liu, Y. Liu, M.-M. Huo, W. Zhang, Recycled indium tin oxide transparent conductive electrode for polymer solar cells, J. Mater. Sci. 55 (2020) 11403–11410.